

Exact four-vector work distribution and covariant Jarzynski's equality for a relativistic particle in an expanding piston

Tingzhang Shi (石霆章)* and Chentong Qi (齐晨桐)*
School of Physics, Peking University, Beijing, 100871, China

H. T. Quan (全海涛)[†]
School of Physics, Peking University, Beijing, 100871, China
Collaborative Innovation Center of Quantum Matter, Beijing 100871, China and
Frontiers Science Center for Nano-optoelectronics, Peking University, Beijing, 100871, China
 (Dated: December 1, 2025)

We investigate the non-equilibrium four-vector work in an expanding relativistic piston. By deriving the exact work distribution in this pedagogical model, we verify the covariant form of Jarzynski's equality. We find that the joint distribution of four-vector work (W^0, W^1) concentrates on the origin and some curves in the (W^0, W^1) space, rather than being smoothly distributed. In the non-relativistic limit, our model consistently recovers the non-relativistic dynamics. We further demonstrate that the momentum component of four-vector work remains significant in both the Lorentz-relativistic and Galilean-relativistic frameworks. In addition, we introduce a novel geometrical technique for analyzing the dynamics of relativistic collision processes, which can be straightforwardly extended to three-dimensional piston models.

I. INTRODUCTION

Covariance is the fundamental requirement for a physical theory. However, the unification of special relativity and thermodynamics has been a longstanding conundrum [1]. On the one hand, the covariant generalizations of the laws of thermodynamics are not so straightforward [2–5]. Some thermodynamic relations, such as the Carnot theorem, have not been generalized to a covariant form. Fortunately, stochastic thermodynamics provides a new perspective on the covariance principle in thermodynamics. Unlike the second law of thermodynamics or the Carnot theorem, which are inequalities, the fluctuation theorems, which are a family of equalities valid for arbitrary non-equilibrium processes [6], could be generalized to the covariant forms without ambiguity [7]. On the other hand, the lack of exactly solvable models, due to the absence of action at a distance in special relativity, makes it difficult to verify the theories of relativistic thermodynamics explicitly. One cannot freely choose a time-dependent potential to perform work on a particle (as we usually do in the non-relativistic stochastic thermodynamics). Luckily, the elastic piston model [8–13] is an ideal choice for relativistic dynamics. The elastic collision is a purely local interaction, and we do not need to introduce any fields to characterize the process of interaction, which significantly simplifies the details of the dynamics.

In a previous work [9], we (two of us and a collaborator) generalized the piston model in Ref. [8] to a special relativistic setting, and verified Jarzynski's equality (JE) [14] in relativistic regime. In the low speed and low

temperature limit, we recovered the results in Ref. [8]. However, the observer is fixed in the laboratory frame of reference. Hence, both the work distribution and the JE do not satisfy the principle of covariance [8, 9].

In this article, in order to investigate the fluctuation theorem in a covariant form, we consider an arbitrary inertial observer. We analytically compute the four-vector work distribution and verify the covariant Jarzynski's equality (JE) [7, 14] in the one-dimensional relativistic piston model. In this relativistic covariant setting, we consider the joint distribution of both the energy and momentum change of the particle due to the elastic collision with the two boundaries of the cylinder. We develop a new geometric method to solve the motion of the particle, and obtain analytical results of the four-vector work distribution. We also find that although the distributions of four-vector work for different inertial observers are different, they all satisfy the same covariant JE [7]. Hence, we demonstrate the covariance principle of fluctuation theorem in this pedagogical model.

The article is organized as follows: In Sec. II, we introduce a novel coordinate transformation technique to calculate the trajectory of the particle. In Sec. III, we analytically calculate the four-vector work distribution of a relativistic particle in an expanding piston system and demonstrate the validity of the covariant JE for an arbitrary inertial observer. We also find that the joint distribution of the four-vector work $W^\mu = (W^0, W^1)$ concentrates on the origin and some curves in the (W^0, W^1) space. In Sec. IV, we give the discussion and summary.

II. A GEOMETRIC METHOD FOR SOLVING THE RELATIVISTIC PISTON MODEL

The model we consider here is a single relativistic classical particle inside a one-dimensional cylinder [8–13], see

* Equal contribution
[†] htquan@pku.edu.cn

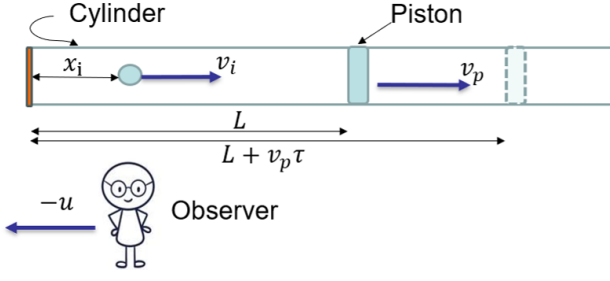


FIG. 1: A relativistic particle moving in a one-dimensional cylinder. The left boundary is fixed in the laboratory reference frame, while the right boundary is a elastic piston with constant velocity v_p . An inertial observer is moving relative to the laboratory frame with a constant velocity $-u$. The initial position and velocity of the particle are x_i and v_i , respectively.

FIG. 1. The mass of the particle m is set to be $m = 1$. In the cylinder's frame, the initial length of the vessel is L , and the gas is initially at the inverse temperature β , where $\beta = 1/(k_B T)$, k_B is the Boltzmann constant, and T is the temperature perceived from the cylinder's frame. We now fix the left boundary and expand the right boundary outwards at the speed v_p , and stop it after a time interval τ . In the following discussion, we denote the left boundary as the cylinder, and the moving boundary on the right as the piston. The particle undergoes several elastic collision with the piston and the cylinder, which means that in the piston's frame, the energy of the particle is a constant, and the direction of the momentum is reversed.

It is worth pointing out that the initial state and the time interval τ are both defined in the cylinder's frame, therefore, the initial canonical ensemble is chosen from a space-like hypersurface which is orthogonal to the worldline of the cylinder (see FIG.2). Especially, when we discuss the covariance of this model, we may introduce an arbitrary inertial frame of reference, in which the initial state is no longer sampled from an isochronous surface (due to the relativity of simultaneity). If we denote the velocity of this arbitrary observer as $-u$, then in this observer's frame, the velocity of the cylinder becomes u , and the velocity of the piston becomes $w = (u + v_p)/(1 + uv_p)$. In special relativity, the transformation of the velocity could be re-expressed with the transformation of the rapidity in a more elegant form. In special relativity, rapidity is the inverse hyperbolic tangent of the velocity (in units of the speed of light c). If we choose the natural unit that $c = 1$, then we could define the rapidity of u and v_p as $y_u = \text{arctanh}(u)$, $y_p = \text{arctanh}(v_p)$. In a Lorentz transformation, the rapidity is directly summed up, $w = \tanh(y_p + y_u)$.

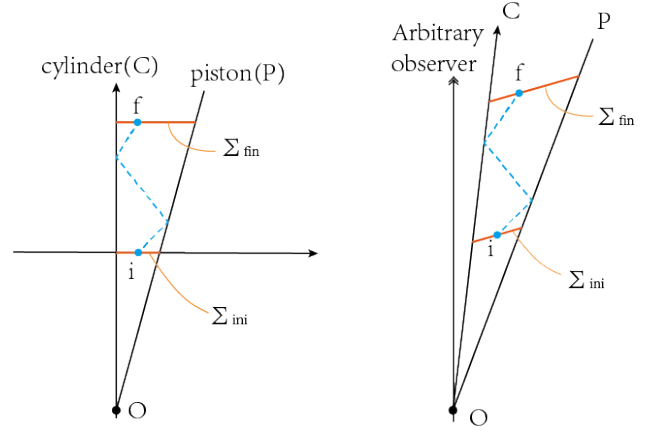


FIG. 2: Worldline of a particle. (Left) The dashed line denotes the worldline of a particle. Line P is the worldline of the piston. In the cylinder's frame, the worldline of the cylinder (Line C) coincides with the time axis (t -axis). An initial state i lies on the x -axis, which is a space-like hypersurface (Σ_{ini}) orthogonal to worldline C . The corresponding final state f also lies on a space-like hypersurface (Σ_{fin} , which represents the isochronous surface $t = \tau$ in the cylinder's frame). (Right) In an arbitrary inertial observer's frame, the initial states no longer belong to any isochronous surface. However, the relation that $\Sigma_{\text{ini}}/\Sigma_{\text{fin}}$ being orthogonal to the line C is still valid.

A. Trajectory of a Single Particle

In the appendix of the related work Ref. [9], a transformation of the worldline has been introduced. The basic idea is to convert the polygonal worldlines into a straight auxiliary worldline, which transforms the restricted motions between boundaries into free motions [15]. In this article, we further discuss the physical meaning of the transformation.

In relativity, a measurement of a component of a Lorentz four-vector gives the inner product of the four-vector and a conjugate unit vector. In this article, the metric tensor is chosen as $\eta_{\mu,\nu} = \eta^{\mu,\nu} = \text{diag}\{1, -1\}$. For the piston with four-velocity $u_p^\mu = (1 - v_p^2)^{-1/2} \cdot (1, v_p)$, the covariant unit vector used to measure the momentum is a unit vector $n_{\mu,p} = (1 - v_p^2)^{-1/2} \cdot (-v_p, 1)$, which is orthogonal to the worldline of the piston. The covariant unit vector to measure energy is simply $u_{\mu,p} = \eta_{\mu\nu} u_p^\nu = (1 - v_p^2)^{-1/2} \cdot (1, -v_p)$. For a particle with four-velocity u_{k-1}^μ before the k -th collision with the piston, the energy and momentum of the particle measured from the piston is

$$\begin{aligned} \mathbb{E}_{k-1} &= m u_{k-1}^\mu \cdot u_{\mu,p}, \\ \mathbb{P}_{k-1} &= m u_{k-1}^\mu \cdot n_{\mu,p}, \end{aligned}$$

and the four-momentum of the particle before the colli-

sion could be re-expressed as

$$P_{k-1}^\mu = mu_{k-1}^\mu = \mathbb{E}_{k-1}u_p^\mu + \mathbb{P}_{k-1}n_p^\mu.$$

After the collision, the energy component remains $\mathbb{E}_k = \mathbb{E}_{k-1}$, and the momentum component is reversed to $\mathbb{P}_k = -\mathbb{P}_{k-1}$, therefore the four momentum after the collision becomes

$$P_k^\mu = \mathbb{E}_k u_p^\mu + \mathbb{P}_k n_p^\mu = mu_{k-1}^\mu = \mathbb{E}_{k-1}u_p^\mu - \mathbb{P}_{k-1}n_p^\mu.$$

An orthogonal reflection with respect to a hypersurface Σ is the map that transform any Lorentz vector χ to a new vector χ' whose orthogonal component relative to Σ is reversed, while its tangential component is preserved. A collision with the piston serves as an orthogonal reflection with respect to the hypersurface P . Since the orthogonal reflection is an involution, we may perform an extra auxiliary orthogonal reflection to preserve the four-velocity of the particle, i.e., the original four-velocity before the collision and the auxiliary four-velocity after the collision is the same. Therefore, the original worldline segment and the auxiliary worldline segment together form a single straight line (see FIG. 3). This framework generalizes the mirror reflection technique in the appendix of Ref. [9], which is still valid when the reference hypersurface is not the t -axis. In this framework, we no longer need to do a Lorentz boost to the piston's frame of reference.

An orthogonal reflection keeps the space-time interval. For a reflection with respect to a time-like hypersurface Σ whose normal four-vector is n , a Lorentz-vector $\chi = \chi_n n + \chi_u u$ will be reflected to $\chi' = -\chi_n n + \chi_u u$. Here u is orthogonal to n and $u_\mu \cdot n^\mu = 0$. The Minkowski inner products of χ and χ' satisfy:

$$\begin{aligned} \chi_\mu \cdot \chi^\mu &= (\chi_n n_\mu + \chi_u u_\mu) \cdot (\chi_n n^\mu + \chi_u u^\mu) \\ &= -\chi_n^2 + \chi_u^2 = -(-\chi_n)^2 + \chi_u^2 \\ &= (-\chi_n n_\mu + \chi_u u_\mu) \cdot (-\chi_n n^\mu + \chi_u u^\mu) \\ &= \chi'_\mu \cdot \chi'^\mu. \end{aligned}$$

If we choose the vector χ to be the space-time separation between an event and a point on the hypersurface, then the space-time interval of the separation is a constant.

During multiple collisions, we may introduce multiple orthogonal reflections with respect to either the (auxiliary) hypersurface C_k (denoting the k -th collision with the cylinder) or the (auxiliary) hypersurface P_k (denoting the $(k+1)$ -th collision with the piston). For example, after the first collision with the piston, we introduce the first auxiliary worldline of C as C_1 . Then, to deal with the second collision between the auxiliary worldline of the particle and C_1 , we perform the second orthogonal reflection with respect to C_1 , which maps P to the second auxiliary worldline P_1 . If the third collision with P_1 happens, the third reflection with respect to P_1 will similarly reflect C_1 to C_2 . If we denote the original worldline as C_0 and P_0 (for unification), then the reflection with respect to C_k maps P_{k-1} to P_k , and the reflection with

respect to P_k maps C_k to C_{k+1} . If the particle collides with the cylinder first, we reflect P_0 with respect to C_0 . If we follow the same rule to label the auxiliary worldline of C and P , we may label the reflection of P_0 with respect to C_0 as P_{-1} . Similarly, we may reflect C_0 with respect to P_{-1} to obtain C_{-1} , reflect P_{-1} with respect to C_{-1} to obtain P_{-2} , and so on (see FIG. 3).

For any preimage e_0 event, the image after the k -th reflection is denoted as e_k (if the first reflection is a reflection with respect to C_0 , and the total number of reflections is $|k|$, we convent the order of the image is $k = -|k|$).

The intersection between C and P is the fixed point during the reflections, which is denoted as O . O lies on every reflection surface, therefore the space-time separation between O and a preimage e_0 equals the space-time separation between O and an arbitrary k -th order image e_k . Especially, if we choose the preimage events as the intersections of Σ_{fin} and the worldline C_0 and P_0 , and denote them as $C_{f,0}/P_{f,0}$, and their k -th order images as $C_{f,k}/P_{f,k}$, then we will find that

$$\begin{aligned} OC_{f,0} \cdot OC_{f,0} &= OC_{f,k} \cdot OC_{f,k}, \\ OP_{f,0} \cdot OP_{f,0} &= OP_{f,k} \cdot OP_{f,k}. \end{aligned}$$

As a result, every $C_{f,k}/P_{f,k}$ lies on a hyperbolic surface centered at O . We denote the hypersurfaces as Σ_C and Σ_P , and the Minkowski distances between Σ_C/Σ_P and O are

$$\begin{aligned} S_C = |OC| &= \tau + \frac{L}{v_p}, \\ S_P = |OP| &= \sqrt{1 - v_p^2} \left(\tau + \frac{L}{v_p} \right). \end{aligned} \quad (1)$$

This treatment is similar to the hyperbolic coordinate techniques introduced in Ref. [16].

The slope of the auxiliary worldline could be determined as follows: an orthogonal reflection keeps the absolute value of the relative rapidity. If we denote the rapidity of the piston to be $y_p = \text{arctanh}(v_p)$, then, for the first collision with the piston, the corresponding rapidity of the auxiliary worldline C_1 is $2y_p$. Similarly, the rapidity of the auxiliary P_1 is $3y_p$. By performing the transformation multiple times, we conclude that the rapidity of C_k is $2ky_p$, and the rapidity of P_k is $(2k+1)y_p$.

The image $C_{f,k}$ is the intersection between Σ_C and C_k , while the image $P_{f,k}$ is the intersection between Σ_P and P_k . Therefore, for the k -th auxiliary $C_{f,k}/P_{f,k}$, the temporal coordinate $t(C_{f,k})/t(P_{f,k})$ and spatial coordinate $x(C_{f,k})/x(P_{f,k})$ are

$$\begin{aligned} [t(C_{f,k}), x(C_{f,k})] &= S_C [\cosh(2ky_p), \sinh(2ky_p)], \\ [t(P_{f,k}), x(P_{f,k})] &= S_P [\cosh((2k+1)y_p), \sinh((2k+1)y_p)]. \end{aligned} \quad (2)$$

The coordinates of the auxiliary $C_{f,k}/P_{f,k}$ could be used to determine the total number of collisions.

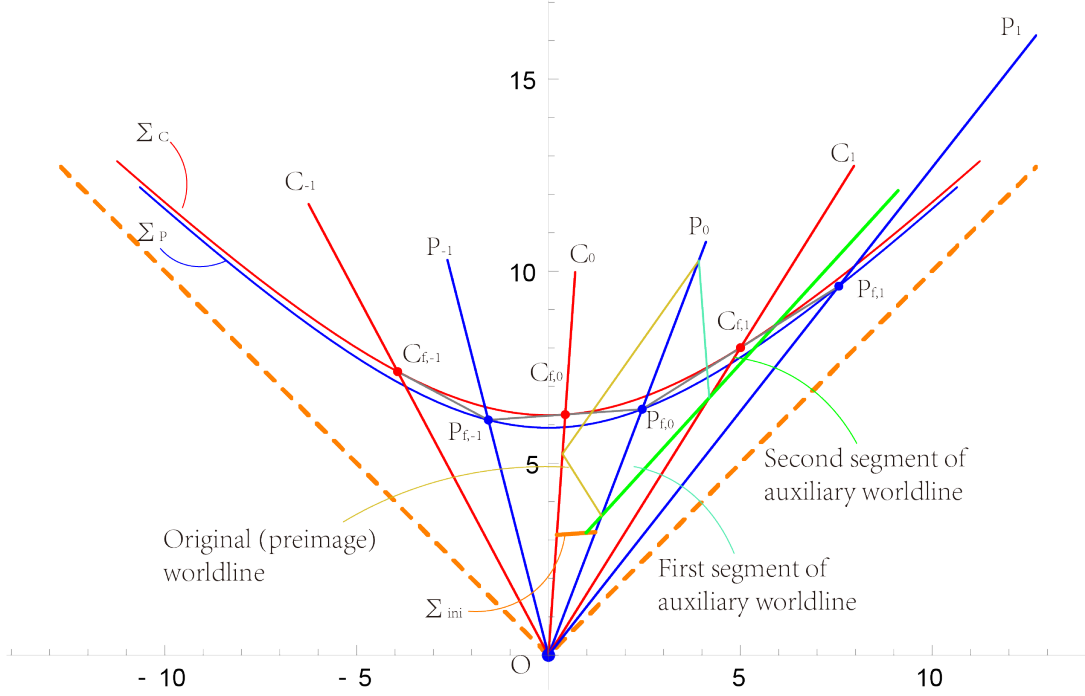


FIG. 3: Orthogonal reflection and auxiliary worldline. This figure demonstrates the original worldline segments and the single straight auxiliary worldline after multiple orthogonal reflections. It also shows the results of the reflections of C_k 's and P_k 's. Meanwhile, the hyperbolas Σ_C , Σ_P denote the events that shares the same space-time interval relative to O . The intersection between C_k and Σ_C is $C_{f,k}$, and the intersection between P_k and Σ_P is $P_{f,k}$, which are denoted by the red and blue dots. In this figure, the velocity $-u$ of the observer is nonzero, therefore, C_0 does not coincide with the t -axis. For the same reason, the Σ_{ini} is no longer isochronous.

For an observer moving with velocity $-u$ relative to the cylinder, we may simply perform a Lorentz transformation centered at O with the rapidity $y_u = \text{arctanh}(u)$, and the influence is to boost the rapidity of every (auxiliary) worldline with the rapidity ny_p to a new (auxiliary) worldline with the rapidity $y_u + ny_p$ (see FIG. 3). The space-time interval is invariant under a Lorentz transformation, therefore S_C/S_P are unchanged. The intersections between the auxiliary worldline and Σ_C/Σ_P are thus boosted to

$$\begin{aligned} & [t(C_{f,k}), x(C_{f,k})] \\ &= S_C[\cosh(2ky_p + y_u), \sinh(2ky_p + y_u)], \\ & [t(P_{f,k}), x(P_{f,k})] \\ &= S_P[\cosh((2k+1)y_p + y_u), \sinh((2k+1)y_p + y_u)]. \end{aligned} \quad (3)$$

These points determines the boundary of (auxiliary) Σ_{fin} , and correspondingly, the Σ_{ini} is also transformed to another space-like hypersurface. Denote the intersection between Σ_{ini} and C (and P) as $C_i : L/v_p[1, 0]$ (and $P_i : \sqrt{1 - v_p^2}L/v_p[\cosh(y_p), \sinh(y_p)]$), then the transformed boundary becomes $C_i : L/v_p[\cosh(y_u), \sinh(y_u)]$ and $P_i : \sqrt{1 - v_p^2}L/v_p[\cosh(y_p + y_u), \sinh(y_p + y_u)]$ (see FIG. 3).

B. Classification of the Number of Collisions in the State Space

For a particle that collides with the piston first, if the initial velocity is $v_i = \tanh(y_i)$, here y_i is the initial rapidity, then the rapidity after the n -th collision is

$$y_n = \begin{cases} y_i - 2ky_p, & n = 2k \\ -y_i + 2ky_p + 2y_u, & n = 2k - 1. \end{cases} \quad (4)$$

If a particle collide with the cylinder first, the rapidity after the first collision is $-y_i + 2y_u$, which satisfies the expression of $y_n|_{n=-1}$. Therefore, we adopt the convention that if the particle collides with the cylinder first, we take the negative number of the collision time as the effective n in the expression of final rapidity.

Once we know the initial state (position and velocity) and the number of collisions, we can deduce the final state of the particle. The key question in deriving the dynamics of this collision model is to determine the number of collisions for a given protocol and initial state. This classification can also be done geometrically with the auxiliary worldline.

In case that the particle happen to collide exactly n times with the boundaries, the (auxiliary) final state must lie on the segment $C_{f,k} - P_{f,k}$ if $n = 2k$, or on the segment $P_{f,k-1} - C_{f,k}$ if $n = 2k - 1$. We denote the final

(auxiliary) space-like hypersurface as $\Sigma_{\text{fin},n}$. If we hope to classify the state space ($x - v$ space) into regions of different collision numbers, then for a given initial velocity v_i , we must figure out what is the range of the initial position allowed for the particle that ensures the particle stops on $\Sigma_{\text{fin},n}$. The procedure is simple: We project the (auxiliary) final hypersurface $\Sigma_{\text{fin},n}$ along the initial velocity v_i onto the initial hypersurface Σ_{ini} . The region projected on Σ_{ini} is the allowed initial position for the particle to end up on $\Sigma_{\text{fin},n}$. This projection is like the “shadow” of $\Sigma_{\text{fin},n}$ under a “parallel light” whose direction is determined by the initial velocity v_i (see FIG. 4). The left and right boundaries of the “shadow” separate the initial state space into regions D_n with different numbers of collisions n (see FIG. 5). When we hope to calculate the distribution function, we can do integration on different state space regions separately.

The overlap between the “shadow” and Σ_{ini} is a time-like hypersurface. In this (1+1) dimensional model, the hypersurface is simply a line segment (in FIG. 4, the black segment, which is the set of all possible initial positions, is the overlap here). We denote the Minkowski’s length of the space-like line segment as the overlap function $\varphi_n(v_i)$ [9] for a given initial velocity v_i . We would like to emphasize that the solution to the motion of the particle is encoded in this overlap function.

For a given number of collisions, the four-vector trajectory work does not depend on the initial position, thus when we calculate the expectation value in the state space and do the integration over the spatial component, we usually encounter the overlap function. The overlap function is a Lorentz scalar, therefore we may apply it safely when we calculate the measure of probability. For

a moving observer, we may perform a backward Lorentz transformation to the cylinder’s frame and calculate this Lorentz scalar.

In the cylinder’s frame, for an even number of collisions $n = 2k$, the $2k$ -th image of Σ_{fin} is the line segment $C_{f,k} - P_{f,k}$ (see FIG. 5). With the coordinates of the boundary points of $\Sigma_{\text{fin},n}$ in Eq. (2), the boundaries of the “shadow” is denoted as the line segment $\xi_{C,k} - \xi_{P,k}$, with coordinates

$$\begin{aligned} [t(\xi_{C,k}), x(\xi_{C,k})] &= \left[0, x(C_{f,k}) - v_i(t(C_{f,k}) - \frac{L}{v_p}) \right], \\ [t(\xi_{P,k}), x(\xi_{P,k})] &= \left[0, x(P_{f,k}) - v_i(t(P_{f,k}) - \frac{L}{v_p}) \right], \end{aligned} \quad (5)$$

and the overlap function [9] is the length of the intersection between the “shadow” and Σ_{ini} , which equals the length $l([0, L] \cap [x(\xi_{C,k}), x(\xi_{P,k})])$, here $l(A)$ represents the length, or the measure, of set A . For an odd number of collisions $n = 2k - 1$, the $(2k - 1)$ -th image of Σ_{fin} becomes the line segment $P_{f,k-1} - C_{f,k}$ (see FIG. 5). The corresponding “shadow” of Σ_{fin} becomes the line segment $\xi_{P,k-1} - \xi_{C,k}$, whose coordinates are given in Eq. (5). The overlap function equals the length $l([0, L] \cap [x(\xi_{P,k-1}), x(\xi_{C,k})])$.

To conclude, the overlap function is

$$\varphi_n(v_i) = \begin{cases} l([0, L] \cap [x(\xi_{C,k}), x(\xi_{P,k})]) & , n = 2k \\ l([0, L] \cap [x(\xi_{P,k-1}), x(\xi_{C,k})]) & , n = 2k - 1. \end{cases} \quad (6)$$

With Eqs. (1), (2), and (5), we derive the explicit expressions as:

$$\begin{aligned} \varphi_{2k-1}(v_i) &= \begin{cases} L - S_P \sinh((2k-1)y_p) + v_i(S_P \cosh((2k-1)y_p) - \frac{L}{v_p}), \\ v_i \in \left[\frac{S_P \sinh((2k-1)y_p) - L}{S_P \cosh((2k-1)y_p) - L \cdot v_p^{-1}}, \frac{S_P \sinh((2k-1)y_p)}{S_P \cosh((2k-1)y_p) - L \cdot v_p^{-1}} \right]; \\ L, \\ v_i \in \left[\frac{S_P \sinh((2k-1)y_p)}{S_P \cosh((2k-1)y_p) - L \cdot v_p^{-1}}, \frac{S_C \sinh(2ky_p) - L}{S_C \cosh(2ky_p) - L \cdot v_p^{-1}} \right]; \\ S_C \sinh(2ky_p) - v_i(S_C \cosh(2ky_p) - \frac{L}{v_p}), \\ v_i \in \left[\frac{S_C \sinh(2ky_p) - L}{S_C \cosh(2ky_p) - L \cdot v_p^{-1}}, \frac{S_C \sinh(2ky_p)}{S_C \cosh(2ky_p) - L \cdot v_p^{-1}} \right]; \end{cases} \\ \varphi_{2k}(v_i) &= \begin{cases} L - S_C \sinh(2ky_p) + v_i(S_C \cosh(2ky_p) - \frac{L}{v_p}), \\ v_i \in \left[\frac{S_C \sinh(2ky_p) - L}{S_C \cosh(2ky_p) - L \cdot v_p^{-1}}, \frac{S_C \sinh(2ky_p)}{S_C \cosh(2ky_p) - L \cdot v_p^{-1}} \right]; \\ L, \\ v_i \in \left[\frac{S_C \sinh(2ky_p)}{S_C \cosh(2ky_p) - L \cdot v_p^{-1}}, \frac{S_P \sinh((2k+1)y_p) - L}{S_P \cosh((2k+1)y_p) - L \cdot v_p^{-1}} \right]; \\ S_P \sinh((2k+1)y_p) - v_i(S_P \cosh((2k+1)y_p) - \frac{L}{v_p}), \\ v_i \in \left[\frac{S_P \sinh((2k+1)y_p) - L}{S_P \cosh((2k+1)y_p) - L \cdot v_p^{-1}}, \frac{S_P \sinh((2k+1)y_p)}{S_P \cosh((2k+1)y_p) - L \cdot v_p^{-1}} \right]. \end{cases} \end{aligned} \quad (7)$$

For a moving observer, we only need to replace the initial velocity v_i with $\tanh(\text{arctanh}(v_i) - \text{arctanh}(u))$, which is

the initial velocity of the same particle, but measured in the cylinder’s frame.

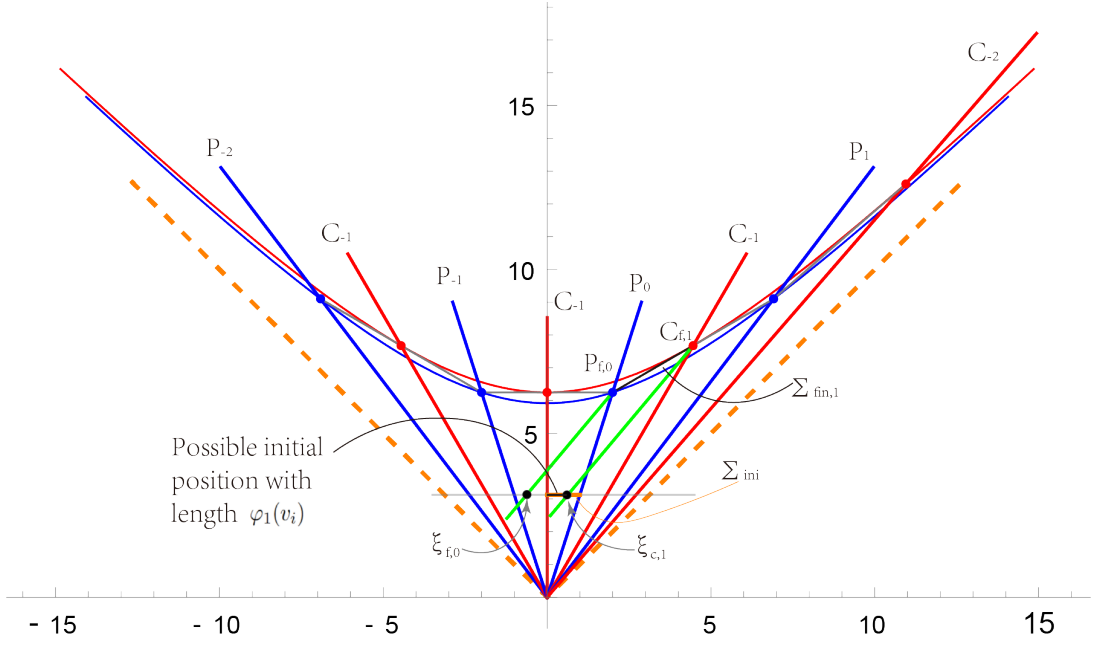


FIG. 4: The “shadow” of $\Sigma_{\text{fin},n}$ on Σ_{ini} is the possible initial position for a particle with initial velocity v_i to collide n times. The “parallel light” is represented by the green lines, and the slope of the “parallel light” is determined by v_i . In this example, the boundaries of the first “shadow” is $\xi_{P,0}(v_i)$ and $\xi_{C,1}(v_i)$, which depend on the velocity of the “parallel light”. They determine the spatial boundaries of domain D_n in the state space. The Minkowski’s length of the “shadow” projected on Σ_{ini} is a Lorentz scalar, therefore we may calculate this value in the laboratory reference frame ($u = 0$).

With the expression of the boundaries of the “shadow”, i.e., Eq. (5), we may separate the state space (x_i, v_i) into different regions D_n with different numbers of collisions n , see FIG. 5. For a given initial velocity and position, we could locate the position of the state in D_n and find the number of collisions. The dynamics of the piston model is completely solved by this geometrical method. The overlap function shows the fraction of the initial position that collide exactly n times for a given initial velocity v_i , which is helpful in calculating ensemble average.

III. FOUR-VECTOR WORK DISTRIBUTION AND COVARIANT JARZYNSKI EQUALITY

A. Lorentz Covariant Work Distribution

In this relativistic case, the initial state satisfies Maxwell-Jüttner distribution at the inverse temperature β [17]

$$F_p(x', p') = \frac{1}{2K_1(\beta mc^2)L} e^{-\beta mc^2 \sqrt{1 + (\frac{p'}{mc})^2}}, \quad (8)$$

where K_1 is the modified Bessel function of the second kind, (x', p') the initial position and momentum of the given particle observed from the cylinder-static frame. This distribution is equivalent to the following

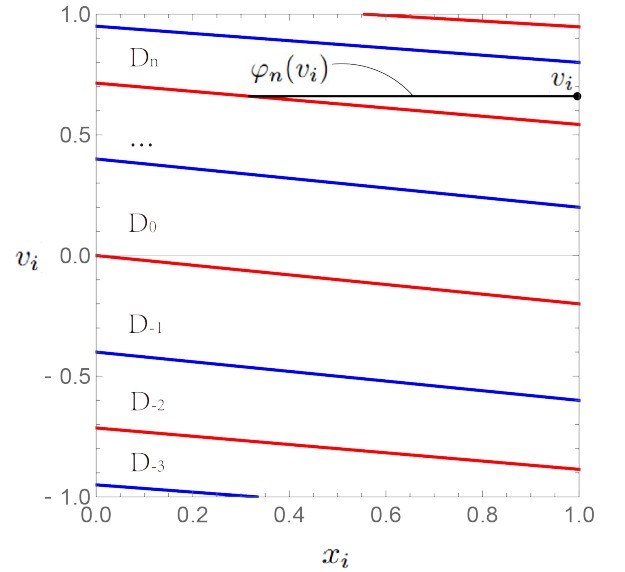


FIG. 5: Separation of domain D_n and the physical meaning of the overlap function $\varphi_n(v_i)$.

distribution expressed in the position-rapidity space.

$$f(x', y'_i) = \frac{1}{2K_1(\beta)L} \cosh(y'_i) e^{-\beta \cosh(y'_i)}. \quad (9)$$

Lorentz transformation gives the relation $y'_i = y_i - y_u$, and thus, the prescription for calculating the four-work distribution reads

$$P_L(W^0, W^1) = \int_0^L dx' \int_{-\infty}^{\infty} dy_i \frac{\exp(-\beta \cosh(y_i - y_u))}{2K_1(\beta)} \times \cosh(y_i - y_u) \delta(W^0 - W_\tau^0(x, y_i)) \delta(W^1 - W_\tau^1(x, y_i)), \quad (10)$$

where the subscript L in $P_L(W^0, W^1)$ stands for the Lorentz covariance.

The four-vector work done by the particle that has collided n times with both the piston and the cylinder wall in the given time period τ is

$$W_\tau^0 = \begin{cases} 2 \sinh(y_i - ky_p) \sinh(ky_p), & n = 2k \\ 2 \sinh(ky_p + y_u) \sinh(y_i - y_u - ky_p), & n = 2k - 1 \end{cases} \quad (11)$$

$$W_\tau^1 = \begin{cases} 2 \cosh(y_i - ky_p) \sinh(ky_p), & n = 2k \\ 2 \cosh(ky_p + y_u) \sinh(y_i - y_u - ky_p), & n = 2k - 1. \end{cases} \quad (12)$$

The above expressions indicate that the zeroth component of the four-vector work is the energy change in classical cases, and the rest three components stand for the classical momentum change.

Utilizing the results obtained in the previous discussion, the integration can be separated into different parts according to the collision count, analytically expressed as

$$P_L(W^0, W^1) = \sum_n \int_{D_n} dx' dy_i \frac{\exp(-\beta \cosh(y_i - y_u))}{2K_1(\beta)} \times \cosh(y_i - y_u) \delta(W^0 - W_\tau^0(x, y_i)) \delta(W^1 - W_\tau^1(x, y_i)). \quad (13)$$

$$P_n(W^0) = \int_{D_n} dy_i \frac{\exp(-\beta \cosh(y_i - y_u)) \cosh(y_i - y_u)}{2K_1(\beta)} \varphi_n(\tanh(y_i - y_u)) \delta(W^0 - W_\tau^0(x, y_i)). \quad (16)$$

For n as an odd number (let $n = 2k - 1$ where k is an integer):

$$P_{2k-1}(W^0) = \frac{\varphi_{2k-1}(\tanh(y_i - y_u)) \cosh(y_i - y_u) \exp(-\beta \cosh(y_i - y_u))}{4K_1(\beta) \sinh(ky_p + y_u) \cosh(y_i - y_u + ky_p)}; \quad (17)$$

$$W_\tau^1 = 2 \cosh(ky_p + y_u) \sinh(y_i - y_u - ky_p). \quad (18)$$

Seen in Eq. (11), y_i can be explicitly expressed by W^0 :

$$y_i = y_u + ky_p + \operatorname{arcsinh}\left(\frac{W^0}{2 \sinh(ky_p + y_u)}\right). \quad (19)$$

By substituting y_i in the covariant work distribution, the

Since each part of the integrand is independent of x' , by integrating x' out first and combine the result with the overlap function derived in the previous section, each component of the summation yields

$$\int_{D_n} dy_i \frac{\exp(-\beta \cosh(y_i - y_u)) \cosh(y_i - y_u)}{2K_1(\beta)} \times \delta(W^0 - W_\tau^0(x, y_i)) \delta(W^1 - W_\tau^1(y_i)) \varphi_n(\tanh(y_i - y_u)), \quad (14)$$

where $\varphi_n(\tanh(y_i))$ is the overlap function in Eq. (7).

The remaining calculation involves a Dirac δ function, and in this case, we integrate out the W_τ^0 term first. Notice that for n of different parities, the four-vector work differs from one to another, hence it is necessary to treat odd n and even n separately.

In the following discussion, for simplicity, remark

$$P_L(W^0, W^1) = \sum_n P_n(W^0) \delta(W^1 - W_\tau^1(W^0)), \quad (15)$$

where

explicit expression of this distribution can be obtained. The exact results are shown in Appendix A, see Eq. (A1) and Eq. (A2). It can be concluded from Eq. (A2) that the work distribution lies solely on various straight lines on the (W^0, W^1) space for odd n 's.

For n as an even number (let $n = 2k$ where k is an integer):

$$P_{2k}(W^0) = \frac{\varphi_{2k}(\tanh(y_i - y_u)) \cosh(y_i - y_u) \exp(-\beta \cosh(y_i - y_u))}{4K_1(\beta) \cosh(y_i - ky_p) \sinh(ky_p)}. \quad (20)$$

$$W_\tau^1 = 2 \cosh(y_i - ky_p) \sinh(ky_p). \quad (21)$$

Repeat the previous procedure, y_i can be expressed as a function of W^0 :

$$y_i = \operatorname{arcsinh}\left(\frac{W^0}{2 \sinh(ky_p)}\right) + ky_p, \quad (22)$$

which yields the probability distribution expression (the detailed results are listed in Appendix A, see Eq. (A3) and Eq. (A4)). It can be concluded from Eq. (A4) that the work distribution lies solely on various hyperbolas on the (W^0, W^1) space for even n 's.

A more intuitive representation of the joint work distribution is illustrated in FIG. 6.

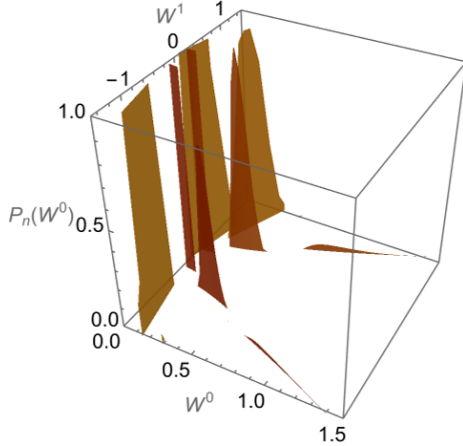


FIG. 6: Four-vector work distribution $P_L(W^0, W^1)$. Here the parameters are chosen to be $L = 1, v_p = 0.1, \tau = 10, \beta = 5$. The height of each sheet denotes the magnitude of the δ function. The work distribution is concentrated on some line segments in the (W^0, W^1) space. The relation between $P_L(W^0, W^1)$ and $P_n(W^0)$ is given in Eq. (15).

For observers with different velocity u , the distribution of work may vary. However, there are some features unchanged for both even and odd numbers of collisions (see FIG. 7). For even n 's, the four-vector work distribution remains lying on the same hyperbolas with the constant spacelike distance to the origin. The positions of the non-zero parts on the hyperbolas change with the velocity of the observer. For odd n 's, the linear relation between W^0 and W^1 remains, only with the slope changed due to the Lorentz transformation. The joint distribution of

four-vector work displays some signatures of the Lorentz covariance: the Lorentz transformation is a linear transformation maintaining the spacetime interval.

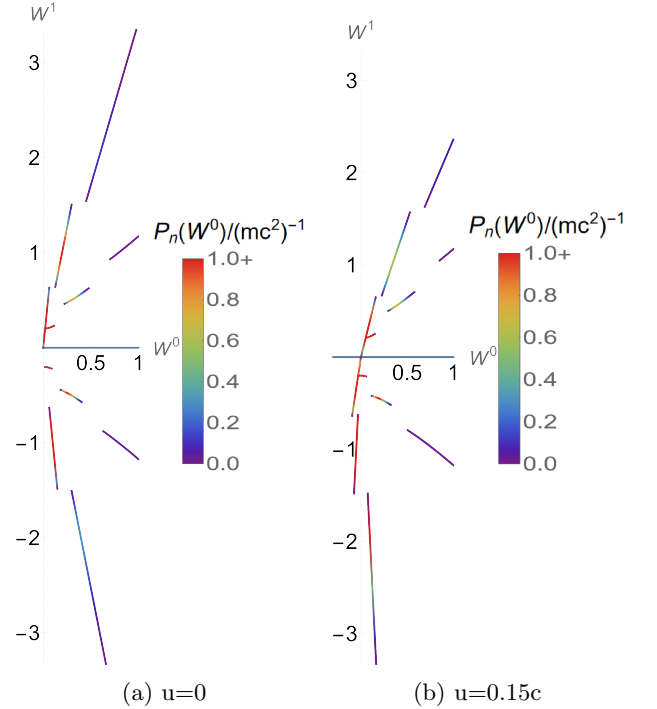


FIG. 7: Joint distribution in different frames of reference. Here the parameters are chosen to be $L = 1, v_p = 0.1, \tau = 10, \beta = 5$. Observers are moving with velocities $-u$ relative to the cylinder. The color of the line denotes $P_n(W^0)$, and the position of the line is determined by $\delta(W^1 - W_\tau^1(W^0))$ in the (W^0, W^1) space. The relation between $P_L(W^0, W^1)$ and $P_n(W^0)$ is given in Eq. (15).

B. Galileo Covariant Work Distribution

Consider a piston model with exactly the same setup, except that the particles are no longer relativistic but obey the Newtonian mechanics.

The dynamics of the system can be resolved by repeating the ‘worldline’ method introduced in the previous section. Given the initial velocity v , the velocity after

colliding n times can be directly derived:

$$v_n = \begin{cases} v_i + 2(k-1)u - 2kw, n = 2k-1 (k \in \mathbb{Z}) \\ v_i + 2ku - 2kw, n = 2k (k \in \mathbb{Z}). \end{cases} \quad (23)$$

The intersection between the worldlines of the piston

and the cylinder wall is $(-Lu(w-u)^{-1}, -L(w-u)^{-1})$. For a particle that collides exactly n times with both the piston and the cylinder wall within time τ , the inverse slope range of the worldlines is $(\tanh(y_u + ny_p), \tanh(y_u + (n+1)y_p))$. Thus, the range of the initial velocity can be expressed as

$$v_i \in \left(\left[\left(\tau + \frac{L}{w-u} \right) (u + nv_p) - \frac{Lu}{w-u} - x \right] \cdot \frac{1}{\tau}, \left[\left(\tau + \frac{L}{w-u} \right) (u + (n+1)v_p) - \frac{Lu}{w-u} - x \right] \cdot \frac{1}{\tau} \right). \quad (24)$$

The domain is thus separated into parallelogram regions

and the overlap function reads

$$\varphi_n(v_i) = \begin{cases} -\left(\tau + \frac{L}{w-u} \right) (u + (n-1)v_p) + \frac{Lw}{w-u} + v_i\tau, \\ v_i \in \left[\left[\left(\tau + \frac{L}{w-u} \right) (u + nv_p) - \frac{Lu}{w-u} \right] \cdot \frac{1}{\tau}, \left[\left(\tau + \frac{L}{w-u} \right) (u + nv_p) - \frac{Lu}{w-u} \right] \cdot \frac{1}{\tau} \right] \\ L, \\ v_i \in \left[\left[\left(\tau + \frac{L}{w-u} \right) (u + nv_p) - \frac{Lu}{w-u} \right] \cdot \frac{1}{\tau}, \left[\left(\tau + \frac{L}{w-u} \right) (u + (n+1)v_p) - \frac{Lu}{w-u} \right] \cdot \frac{1}{\tau} \right] \\ \left(\tau + \frac{L}{w-u} \right) (u + nv_p) - \frac{Lu}{w-u} - v_i\tau, \\ v_i \in \left[\left[\left(\tau + \frac{L}{w-u} \right) (u + (n+1)v_p) - \frac{Lu}{w-u} \right] \cdot \frac{1}{\tau}, \left[\left(\tau + \frac{L}{w-u} \right) (u + (n+1)v_p) - \frac{Lu}{w-u} \right] \cdot \frac{1}{\tau} \right]. \end{cases} \quad (25)$$

In comparison with the relativistic case (Eq. 7), this non-relativistic result is much simpler.

As the particles obey Maxwellian distribution, the work distribution reads

$$P_G(W^0, W^1) = \sum \int dx_i dv_i \frac{\sqrt{\beta} \exp(-\frac{1}{2}(v_i - u)^2)}{\sqrt{2\pi}L} \times \delta(W^0 - W_\tau^0) \delta(W^1 - W_\tau^1), \quad (26)$$

where the subscript G in $P_G(W^0, W^1)$ stands for Galileo covariance.

Denote $P_n(W^0)$ as

$$\int dx_i dv_i \frac{\sqrt{\beta} \exp(-\frac{1}{2}(v_i - u)^2)}{\sqrt{2\pi}L} \delta(W^0 - W_\tau^0), \quad (27)$$

and thus P_G can be expressed as

$$P_G(W^0, W^1) = \sum P_n(W^0) \delta(W^1 - W_\tau^1). \quad (28)$$

By treating odd n and even n separately, this distribution can be expressed analytically.

For n as an odd integer, let $n = 2k-1$. As the integrand is independent of x , by integrating x out first,

P_{2k-1} can be expressed as

$$P_{2k-1}(v_i) = \frac{\sqrt{\beta}}{\sqrt{2\pi}L} \varphi_{2k-1}(v_i) \frac{\exp(-\frac{1}{2}(v_i - u)^2)}{2kw - 2(k-1)u}, \quad (29)$$

and

$$W_\tau^1 = 2v_i - 2kw + 2(k-1)u. \quad (30)$$

Notice that v_i is a function of W^0 :

$$v_i = \frac{W^0 + 2((k-1)u - kw)^2}{2(kw - (k-1)u)}, \quad (31)$$

thus P_{2k-1} can be derived. The exact result is given in Appendix A, see Eq. (A5) and Eq. (A6).

For n as an even integer, let $n = 2k$. The calculation process is similar to the case where n is an odd number, except that the change of momentum is $2kw - 2ku$ due to the fact that v_{2n} points at the same direction as v_i . The exact work distribution for colliding $2k$ times with both the cylinder wall and the piston can be derived, and the exact distribution is given in Appendix A (see Eq. (A7) and Eq. (A8)).

A more intuitive representation of the joint work distribution is illustrated in FIG. 8.

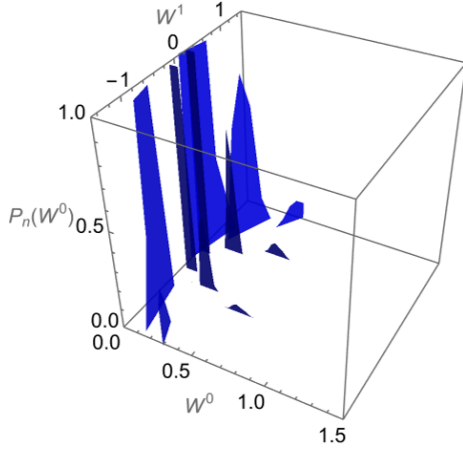


FIG. 8: Four-vector work distribution for non-relativistic particle. Here the parameters are chosen to be $L = 1$, $v_p = 0.1$, $\tau = 10$, $\beta = 5$, $u = 0$. The height of each sheet denotes the magnitude of the δ function. The work distribution is also concentrated on some line segments in the (W^0, W^1) space. The relation between $P_L(W^0, W^1)$ and $P_n(W^0)$ is given in Eq. (28). We can see that on the sheets representing odd numbers of collisions, the W^1 components are some constants, which significantly differs from the special relativistic results.

C. Distribution of Four-vector Work Measured from Different Frames of Reference and the Covariant Jarzynski's Equality

The covariant JE reads [7]

$$\langle e^{\beta_\mu W^\mu} \rangle = e^{-\beta(F_f - F_i)} = \frac{Z_f}{Z_i}, \quad (32)$$

here $\beta_\mu = \beta u_{C,\mu}$ is the four-vector inverse temperature of the initial canonical ensemble [2], u_C is the four-velocity of the cylinder, W^μ is the four-vector work which is the inverse of the change of four-momentum during the driving process (the convention in Refs. [8, 9] and the current article define the work as the work output, which are slightly different from the typical convention [7, 14]), F_i and F_f are the initial and final free energy of the thermal state defined on the hypersurface Σ_{ini} and Σ_{fin} , Z_i and Z_f are the initial and final partition function corresponding to the thermal state on Σ_{ini} and Σ_{fin} .

The partition function is an integration on a space-like hypersurface. In our setup, Z_i and Z_f are [18]

$$Z_{i/f} = \int_{\Sigma_{i/f}} d\Sigma_\mu \frac{P^\mu}{m} \frac{dP^1}{P^0} \exp(-\beta_\mu P^\mu), \quad (33)$$

here $d\Sigma_\mu$ is a space-like surface element on $\Sigma_{i/f}$, P^1 is the momentum of the particle, $P^\mu = (\sqrt{1 + P^{1^2}}, P^1)$ is the four-momentum of the particle's initial state, dP^1/P^0 is the Lorentz invariant measure in the phase space,

$\exp(-\beta_\mu P^\mu)$ is the Jüttner-Synge factor [17–19]. For the thermal state with the same β_μ on Σ_i and Σ_f , we no longer need to compute the details of integration in momentum space. The ratio Z_f/Z_i is simply the ratio between the area Σ_i and Σ_f , and the ratio is $(L + v_p \tau)/L$.

With the analytical expression of the distribution of four-vector work, we can numerically verify JE for an arbitrary moving observer (see FIG.9, FIG.10). In FIG.7, we have shown that the joint distributions of the four-vector work for different inertial observers are related via a Lorentz transformation. The rapidity of each straight line segment is Lorentz boosted by the same value y_u , and the positions of both ends of the nonzero part on each hyperbola are also Lorentz boosted under the same principle (the hyperbolas themselves are fixed because each hyperbola indicates a constant spacetime interval, which is Lorentz invariant). However, the exponent $\beta_\mu W^\mu$ in the covariant JE is a Lorentz scalar. Meanwhile, the probability measure is also a Lorentz scalar. This explains why the expectation value of the exponential work is Lorentz invariant.

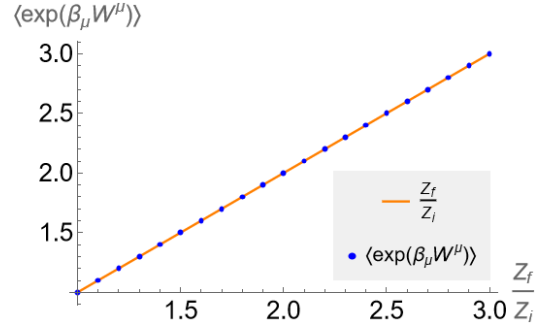


FIG. 9: Expectation value of the exponential four-vector work under different protocols. In this figure, the driving time is changed, thus the ratio between the initial and final length of the vessel (which equals Z_f/Z_i) is changed. The observer is moving with velocity $u = 0.2c$ backwards in the x direction, the inverse temperature in the rest frame of the reservoir is $\beta = 5$, the velocity of the piston in the cylinder's frame is $v_p = 0.1c$. In this numerical calculation, the error of the JE is on the same order of magnitude as the error in the normalization of probability, indicating that the covariant JE is exact.

D. Consistency and Differences between Lorentz and Galileo Covariant Work Distributions

For a relativistic system, when taking the low speed limit, the results attained through relativistic mechanics are expected to coincide with Newtonian mechanics. This remains valid in the relativistic piston model. The Lorentz covariant four-vector work distribution derived in the previous paragraphs is supposed to approach that

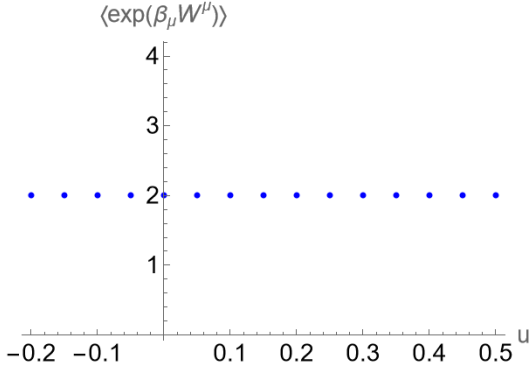


FIG. 10: Expectation value of the exponential four-vector work perceived from different observers. In this figure, the protocol is fixed, thus the ratio between the initial and final length of the vessel (which equals Z_f/Z_i) is fixed to be 2 (by setting $L = 1, v_p = 0.1, \tau = 10$), the inverse temperature in the rest frame of the reservoir is $\beta = 5$. The observers are moving with different u backwards in the x direction. For different observers, although the joint distributions of the four-vector work are different, the expectation value of the exponential four-vector work are exactly the same, demonstrating the validity of the covariant JE.

of the Galileo covariant four-vector work distribution. In the following, we will check this.

To start with, consider the separation of domains. By taking the low speed limit, $\sinh(ny_p)$ in Eq. (7) becomes nv_p , and $\cosh(ny_p)$ becomes 1. Obviously, the separation of domain in Eq. (7) is equivalent to the separation in Eq. (25). As both overlap functions form trapezoidal regions on the $x - v$ plane, this equivalence indicates that the overlap function of the Lorentz covariant case is consistent with the overlap function in the Galileo covariant case.

Next, examine each component of the distribution. Take P_{2k-1} and P_{2k} in the Lorentz covariant distribution. If each counterpart in the Lorentz and Galileo covariant distribution is equivalent to each other, then the consistency between the two covariant models can be verified.

As $\sinh x \approx x \approx \tanh x$ for $|x| \ll 1$, rapidity and velocity can be considered equivalent. As β approaches ∞ , the Bessel function can be approximated as $K_1(\beta) \approx e^{-\beta} \pi^{1/2} (2\beta)^{-1/2}$. This approximation brings an extra β to the exponent in the Lorentz covariant four-vector work distribution.

First, consider P_{2k-1} and its corresponding δ function in the Lorentz covariant case. The Lorentz covariant distribution can be divided into three segments: the exponential part, the δ function part and the rest multiplications. Taking into account the approximation of the Bessel function, the exponential part can be approximated in the following way:

$$\begin{aligned}
 & \exp \left[-\beta \left(\cosh(ky_p) \sqrt{1 + \left(\frac{W^0}{2 \sinh(ky_p + y_u)} \right)^2} + \sinh(ky_p) \frac{W^0}{2 \sinh(ky_p + y_u)} \right) + \beta \right] \\
 & \approx \exp \left[\beta \left(\left(1 + \frac{k^2 y_p^2}{2} \right) \left(1 + \frac{1}{2} \left(\frac{W^0}{2(ky_p + y_u)} \right)^2 + \frac{ky_p W^0}{2(ky_p + y_u)} - 1 \right) \right) \right] \\
 & \approx \exp \left[-\frac{\beta}{2} \left(\frac{W^0}{2(u + kw - ku)} + k(w - u) \right)^2 \right] = \exp \left[-\frac{\beta}{2} \left(\frac{W^0 + 2((k-1)u - kw)^2}{2(kw - (k-1)u)} - u \right)^2 \right].
 \end{aligned} \tag{34}$$

For the δ function segment,

$$\frac{W^0}{\tanh(y_u + ky_p)} \approx \frac{W^0}{kw - (k-1)u}. \tag{35}$$

For the rest of the multipliers, expand the remaining multipliers in the Lorentz covariant distribution to the first order. Notice that v and y are all first order small quantities, while W^0 is approximately proportional to v^2 , making it a second order small quantity. The expansion leads to:

$$\begin{aligned}
& \left(\cosh(ky_p) \sqrt{1 + \left(\frac{W^0}{2 \sinh(y_u + ky_p)} \right)^2} + \frac{\sinh(ky_p) W^0}{2 \sinh(ky_p + y_u)} \right) \cdot \left(2 \sinh(ky_p + y_u) \sqrt{1 + \left(\frac{W^0}{2 \sinh(y_u + ky_p)} \right)^2} \right)^{-1} \\
& \approx \left[\left(1 + \frac{k^2 y_p^2}{2} \right) \left(1 + \frac{1}{2} \left(\frac{W^0}{2(y_u + ky_p)} \right)^2 \right) + \frac{ky_p W^0}{2(ky_p + y_u)} \right] \left(1 - \frac{1}{2} \left(\frac{W^0}{2(kw - (k-1)u)} \right)^2 \right) \cdot \frac{1}{2(kw - (k-1)u)} \\
& \approx \left(1 + \frac{1}{2} k^2 y_p^2 + \frac{ky_p W^0}{2(ky_p + y_u)} \right) \cdot \frac{1}{2(kw - (k-1)u)} \\
& \approx (1 + O(v_i)) \cdot \frac{1}{2(kw - (k-1)u)} \approx \frac{1}{2(kw - (k-1)u)}.
\end{aligned} \tag{36}$$

Multiplying the results yielded in the previous calculations (34–36), it can be concluded that by taking the low speed limit, the Lorentz covariant four-vector work distribution is equivalent to the Galileo covariant four-vector work distribution when the collision count is an odd integer, see Eqs. (A1,A2,A5,A6).

Then, let us consider P_{2k} and its corresponding δ function in the Lorentz covariant case. The three-segments division is still valid in the following discussion. Taking into account the approximation of Bessel function, the exponential part can be approximated in the following way:

$$\begin{aligned}
& \exp \left[-\beta \left(-\frac{W^0 \sinh(y_u - ky_p)}{2 \sinh(ky_p)} + \sqrt{1 + \left(\frac{W^0}{2 \sinh(ky_p)} \right)^2} \cosh(y_u - ky_p) \right) + \beta \right] \\
& \approx \exp \left[-\beta \left(-\frac{W^0(u - k(w - u))}{2k(w - u)} + \left(1 + \frac{1}{2} \left(\frac{W^0}{2k(w - u)} \right)^2 \right) \left(1 + \frac{(u - k(w - u))^2}{2} \right) - 1 \right) \right] \\
& \approx \exp \left[-\frac{\beta}{2} \left(\frac{W^0}{2k(w - u)} + kw - (k+1)u \right)^2 \right] = \exp \left[-\frac{\beta}{2} \left(\frac{W^0 + 2k^2(w - u)^2}{2k(w - u)} - u \right)^2 \right].
\end{aligned} \tag{37}$$

For the δ function segment,

$$2 \sqrt{1 + \left(\frac{W^0}{2 \sinh(ky_p)} \right)^2} \sinh(ky_p) \approx 2ky_p(1 + O(v_i)) \approx 2ky_p \approx 2k(w - u). \tag{38}$$

For the rest of the multipliers, expanding them to the first order leads to:

$$\begin{aligned}
& \left[-\frac{W^0 \sinh(y_u - ky_p)}{2 \sinh(ky_p)} + \sqrt{1 + \left(\frac{W^0}{2 \sinh(ky_p)} \right)^2} \cosh(y_u - ky_p) \right] \cdot \left(2 \sqrt{1 + \left(\frac{W^0}{2 \sinh(ky_p)} \right)^2} \sinh(ky_p) \right)^{-1} \\
& \approx \left(1 - \frac{1}{2} \left(\frac{W^0}{2ky_p} \right)^2 \right) \left[-\frac{W^0(y_u - ky_p)}{2ky_p} + \left(1 + \frac{1}{2} \left(\frac{W^0}{2ky_p} \right)^2 \right) \left(1 + \frac{(y_u - ky_p)^2}{2} \right) \right] \cdot \frac{1}{2ky_p} \\
& \approx \left(1 + \frac{(y_u - ky_p)^2}{2} - \frac{W^0(y_u - ky_p)}{2ky_p} \right) \cdot \frac{1}{2ky_p} \\
& \approx (1 + O(v_i)) \cdot \frac{1}{2ky_p} \approx \frac{1}{2k(w - u)}.
\end{aligned} \tag{39}$$

Multiplying the results yielded in the previous calculations(37–39), it can be concluded that by taking the low speed limit, the Lorentz covariant four-vector work distribution is equivalent to the Galileo covariant

four-vector work distribution when the collision count is an even integer, see Eqs. (A3,A4,A7,A8).

Thus, from the discussion above, the consistency between Lorentz covariance and Galileo covariance in the

low speed limit can be verified.

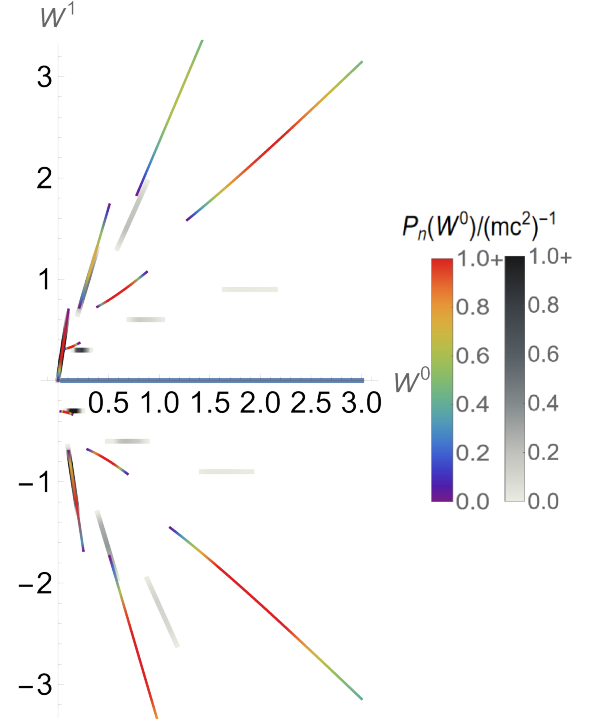
Despite the consistency, the results from the Lorentz and Galileo covariant work distributions also display discrepancies. To identify the conditions under which the deviation is prominent, the two distributions are plotted under different driving velocity and temperature circumstances. From the graphics result (see FIG.11), it can be concluded that the Lorentz covariant results differ more significantly from the Galileo covariant results at high temperature and fast speed.

IV. DISCUSSION AND SUMMARY

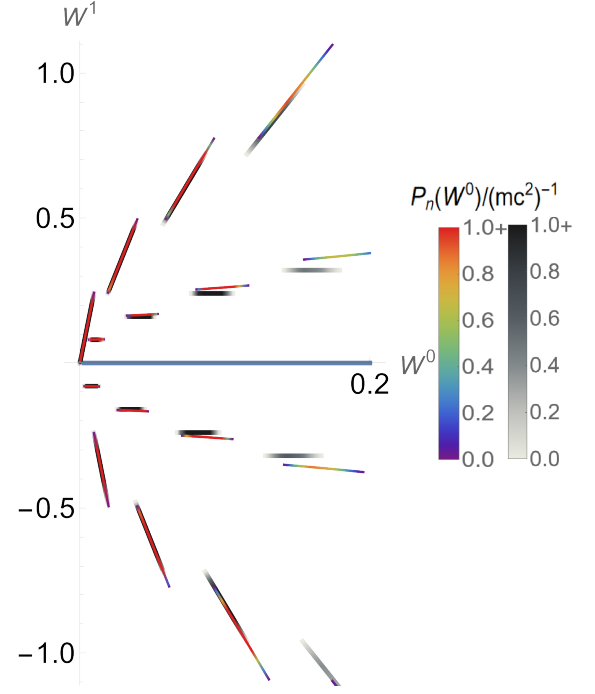
Let us look further into the main results we obtained. We derive the joint distribution of four-vector work perceived by an arbitrary inertial observer. The first feature of the joint distribution function of four-vector work is that the probability concentrate on the origin and some curves in the (W^0, W^1) space, instead of any smooth distribution. The second feature of the distribution is that the concentration line is either linear or hyperbolic, which reflects the main features of Lorentz transformation: The Lorentz transformation is a linear transformation maintaining the space-time interval. We investigate the difference between relativistic and Newtonian mechanics, and find the difference in both the magnitude and the position of the $W^0 - W^1$ line. We also show that the momentum component of the four-vector work contributes significantly to the average exponential work, even in the non-relativistic limit.

Technically, we developed a new method to solve the dynamics of the collision process. The geometrical solution avoids the tedious calculation in the recursion of the time of collisions [9], providing a clear physical intuition of the relativistic collision motion. This method could be generalized to (2+1) dimensional or (3+1) dimensional relativistic piston model directly. For example, in the (2+1) dimensional piston model, the boundary of the vessel is a line, and in Minkowski space, the motion of the line can be described by a worldsheet-like hypersurface. We may still introduce the orthogonal reflection for the hypersurface, which reverses the orthogonal component while maintaining the parallel component with respect to the hypersurface of the boundary. An orthogonal reflection still characterizes an elastic collision, and we may still introduce an extra orthogonal reflection to make sure the auxiliary worldline to be a straight line. Our future work will focus on these generalization to the more realistic models. In 2009, R. Nolte and A. Engel studied the (3+1) dimensional model [20], but the number of collisions is limited to no more than one. Now, with our new geometrical solution, it is possible to investigate a more general protocol, in which multiple collisions are allowed. Our method may also be helpful in solving the motion of classical or quantum Klein-Gordon field with Dirichlet boundary condition [15, 16].

In summary, we study a simple model of a piston and



(a) $Z_f/Z_i = 2.7, v_p = 0.15c, \beta = 1.2$.



(b) $Z_f/Z_i = 2, v_p = 0.04c, \beta = 10$.

FIG. 11: Comparison of the joint distributions of four-vector work for relativistic and non-relativistic dynamics. The parameters are shown below each figure. The thin rainbow-colored curves represent the four-vector work distribution of the relativistic piston model, while the thick curves shaded according to the GrayTones (reversed) scheme corresponds to the non-relativistic piston model. In the low-temperature and slow-driving regime, the relativistic distribution converges toward its non-relativistic counterpart.

ideal gas in the framework of the special theory of relativity. We calculate the four-vector work of a piston system under linear quench perceived by an arbitrary inertial observer. Using a novel coordinate transformation technique, we obtain an analytical result of the joint distribution of four-vector work (A1) - (A4) and verify the covariant JE. With our result, it is possible to observe the deviation of relativistic work distribution (A1) - (A4) from the non-relativistic one (A5) - (A8). In principle, these relativistic corrections become non-negligible in the high-temperature and fast-speed limit. However, the range of parameters where relativistic effects are observable would already be far beyond the current experimental techniques. Our results show that the momentum component in the four-vector work matters in the covariant JE, even in the non-relativistic limit. This model gives a clear example of the covariant JE, thus serving

the pedagogical purpose.

ACKNOWLEDGEMENTS

Chentong Qi thanks Yichen Xiao for helpful discussions.

This work is supported by the National Natural Science Foundations of China (NSFC) under Grants No. 12375028 and No. 12521004.

Appendix A: Exact Result of Lorentz and Galileo Covariant work distributions

In the case of Lorentz covariance, for $n = 2k - 1$ where k is an integer, by replacing y_i in Eqs. (17) and (18) with Eq. (19), the distribution reads:

$$\begin{aligned}
 P_{2k-1}(W^0) = & \varphi_{2k-1} \left[\left(\sinh(ky_p) \sqrt{1 + \left(\frac{W^0}{2 \sinh(ky_p)} \right)^2} + \frac{\cosh(ky_p) W^0}{2 \sinh(ky_p + y_u)} \right) \times \right. \\
 & \left. \left(\cosh(ky_p) \sqrt{1 + \left(\frac{W^0}{2 \sinh(ky_p + y_u)} \right)^2} + \frac{W^0 \sinh(ky_p)}{2 \sinh(y_u + ky_p)} \right)^{-1} \right] \cdot \left(4K_1(\beta) \sinh(ky_p + y_u) \sqrt{1 + \left(\frac{W^0}{2 \sinh(ky_p + y_u)} \right)^2} \right)^{-1} \\
 & \exp \left[-\beta \left(\cosh(ky_p) \sqrt{1 + \left(\frac{W^0}{2 \sinh(ky_p + y_u)} \right)^2} + \frac{\sinh(ky_p) W^0}{2 \sinh(ky_p + y_u)} \right) \right] \\
 & \left(\cosh(ky_p) \sqrt{1 + \left(\frac{W^0}{2 \sinh(ky_p + y_u)} \right)^2} + \frac{\sinh(ky_p) W^0}{2 \sinh(ky_p + y_u)} \right);
 \end{aligned} \tag{A1}$$

$$\delta(W^1 - W_\tau^1(W^0)) = \delta \left(W^1 - \frac{\cosh(y_u + ky_p) W^0}{\sinh(y_u + ky_p)} \right). \tag{A2}$$

For $n = 2k$ where k is an integer, by replacing y_i in

Eqs. (20) and (21) with Eq. (22), the distribution reads:

$$\begin{aligned}
P_{2k}(W^0) = & \varphi_{2k} \left[\left(\sinh(ky_p - y_u) \sqrt{1 + \left(\frac{W^0}{2 \sinh(ky_p)} \right)^2} + \frac{W^0 \cosh(ky_p - y_u)}{2 \sinh(ky_p)} \right) \times \right. \\
& \left. \left(\cosh(ky_p - y_u) \sqrt{1 + \left(\frac{W^0}{2 \sinh(ky_p)} \right)^2} + \frac{W^0 \sinh(ky_p - y_u)}{2 \sinh(ky_p)} \right)^{-1} \right] \\
& \left(-\frac{W^0 \sinh(y_u - ky_p)}{2 \sinh(ky_p)} + \sqrt{1 + \left(\frac{W^0}{2 \sinh(ky_p)} \right)^2} \cosh(y_u - ky_p) \right) \cdot \left(4K_1(\beta) \sqrt{1 + \left(\frac{W^0}{2 \sinh(ky_p)} \right)^2} \sinh(ky_p) \right)^{-1} \\
& \exp \left[-\beta \left(-\frac{W^0 \sinh(y_u - ky_p)}{2 \sinh(ky_p)} + \sqrt{1 + \left(\frac{W^0}{2 \sinh(ky_p)} \right)^2} \cosh(y_u - ky_p) \right) \right];
\end{aligned} \tag{A3}$$

$$\delta(W^1 - W_\tau^1(W^0)) = \delta \left(W^1 - 2 \sqrt{1 + \left(\frac{W^0}{2 \sinh(ky_p)} \right)^2} \sinh(ky_p) \right). \tag{A4}$$

In the case of Galileo covariance, for $n = 2k - 1$ where

k is an integer, by replacing v_i in Eqs. (29) and (30) with Eq. (31), the distribution reads:

$$P_{2k-1}(W^0) = \frac{\sqrt{\beta}}{\sqrt{2\pi}L} \varphi_{2k-1} \left(\frac{W^0 + 2((k-1)u - kw)^2}{2(kw - (k-1)u)} \right) \cdot \exp \left[-\frac{\beta}{2} \left(\frac{W^0 + 2((k-1)u - kw)^2}{2(kw - (k-1)u)} - u \right)^2 \right] \cdot [2(kw - (k-1)u)]^{-1}; \tag{A5}$$

$$\delta(W^1 - W_\tau^1(W^0)) = \delta \left(W^1 - \frac{W^0}{2(kw - (k-1)u)} \right). \tag{A6}$$

For $n = 2k$ where k is an integer, by repeating the

above process, the distribution reads:

$$P_{2k}(W^0) = \frac{\sqrt{\beta}}{\sqrt{2\pi}L} \varphi_{2k} \left(\frac{W^0 + 2k^2(u - w)^2}{2k(w - u)} \right) \cdot \exp \left[-\frac{\beta}{2} \left(\frac{W^0 + 2k^2(u - w)^2}{2k(w - u)} - u \right)^2 \right] \cdot [2k(w - u)]^{-1}; \tag{A7}$$

$$\delta(W^1 - W_\tau^1(W^0)) = \delta(W^1 - 2k(w - u)). \tag{A8}$$

-
- [1] J. Dunkel, P. Hänggi, and S. Hilbert, Non-local observables and lightcone-averaging in relativistic thermodynamics, *Nature Physics* **5**, 741 (2009).
[2] N. G. van Kampen, Relativistic thermodynamics of moving systems, *Phys. Rev.* **173**, 295 (1968).

- [3] N. G. van Kampen, Relativistic thermodynamics, *J. Phys. Soc. Jpn. Suppl.* **26**, 316 (1969).
[4] W. Israel and J. Stewart, Transient relativistic thermodynamics and kinetic theory, *Annals of Physics* **118**, 341 (1979).

- [5] W. Israel, Thermodynamics of relativistic systems, *Physica A: Statistical Mechanics and its Applications* **106**, 204 (1981).
- [6] J.-F. Chen and H. T. Quan, Hierarchical structure of fluctuation theorems for a driven system in contact with multiple heat reservoirs, *Phys. Rev. E* **107**, 024135 (2023).
- [7] J.-H. Pei, J.-F. Chen, and H. T. Quan, Promoting fluctuation theorems into covariant forms, *Phys. Rev. Lett.* **134**, 237102 (2025).
- [8] R. C. Lua and A. Y. Grosberg, Practical applicability of the jarzynski relation in statistical mechanics: A pedagogical example, *J. Phys. Chem. B* **109**, 6805 (2005).
- [9] X. Zhang, T. Shi, and H. T. Quan, Exact work distribution and jarzynski's equality of a relativistic particle in an expanding piston, *Phys. Rev. E* **110**, 024128 (2024).
- [10] H. T. Quan and C. Jarzynski, Validity of nonequilibrium work relations for the rapidly expanding quantum piston, *Phys. Rev. E* **85**, 031102 (2012).
- [11] Z. Fei, J. Zhang, R. Pan, T. Qiu, and H. T. Quan, Quantum work distributions associated with the dynamical casimir effect, *Phys. Rev. A* **99**, 052508 (2019).
- [12] T. Qiu, Z. Fei, R. Pan, and H. T. Quan, Path-integral approach to the calculation of the characteristic function of work, *Phys. Rev. E* **101**, 032111 (2020).
- [13] Z. Gong, Y. Lan, and H. T. Quan, Stochastic thermodynamics of a particle in a box, *Phys. Rev. Lett.* **117**, 180603 (2016).
- [14] C. Jarzynski, Nonequilibrium equality for free energy differences, *Phys. Rev. Lett.* **78**, 2690 (1997).
- [15] G. T. Moore, Quantum theory of the electromagnetic field in a variable-length one-dimensional cavity, *J. Math. Phys.* **11**, 2679 (1970).
- [16] M. Koehn, Solutions of the klein-gordon equation in an infinite square-well potential with a moving wall, *Europhys. Lett.* **100**, 60008 (2013).
- [17] F. Jüttner, Das Maxwellsche Gesetz der Geschwindigkeitsverteilung in der Relativtheorie, *Annalen der Physik* **339**, 856 (1911).
- [18] R. Hakim, *Introduction to Relativistic Statistical Mechanics: Classical and Quantum* (WORLD SCIENTIFIC, 2011).
- [19] J. L. Synge, *The relativistic gas* (North-Holland Publishing Company, Amsterdam; Interscience Publishers Inc., New York, 1957).
- [20] R. Nolte and A. Engel, Jarzynski equation for the expansion of a relativistic gas and black-body radiation, *Physica A: Statistical Mechanics and its Applications* **388**, 3752 (2009).